International Journal of Engineering

Journal Homepage: www.ije.ir

Effects of Ageing and Forging on Short-term Creep Behaviors of Inconel-713C Superalloy at 850 °C

M. Azadi*[a], M. Azadi[b], A. Hajiali Mohammadi[b]

[a] *Faculty of Materials and Metallurgical Engineering, Semnan University, Semnan, Iran*
[b] *Faculty of Mechanical Engineering, Semnan University, Semnan, Iran*

PAPER INFO

Paper history:
Received 26 January 202
Received in revised form 03 February 2020
Accepted 06 March 2020

Keywords:
Inconel-713C Superalloy
Short-term Creep
Age-hardening
Forging
Microstructure

ABSTRACT

In this paper, the short-term creep behavior of the Inconel-713C superalloy after different pre-treatments including the ageing and forging processes has been studied at 850 °C. The ageing heat treatment was heating at 930 °C for 16 hours without solutioning process. The optical microscopy (OM) and the scanning electron microscopy (SEM) techniques were applied for microstructural evaluations. The results showed that although the ageing treatment increased the γ' phase content, the age-hardened material had a lower creep lifetime (about 40%) with respect to *the* as-cast alloy. This was related to the decrease in the amount of $M_{23}C_6$-type secondary carbides precipitation. When the Inconel-713C superalloy specimen was forged at 1200 °C, the third stage of the creep curve (strain versus time) increased drastically and shortened the creep lifetime. The small grain size of the forged specimen was responsible for such inverse creep behavior. In addition, fractographs of this specimen indicated intragranular cracks on the ruptured surface. When the forged sample was age-hardened directly without the solutioning treatment, the creep lifetime increased about 4 times as compared to the forged specimen.

***doi**: 10.5829/ije.2020.33.04a.15*

1. INTRODUCTION

The Inconel-713C nickel-based superalloy tolerates hard and complex operating conditions such as high temperatures, temperature gradients, abrupt thermal changes, the oxidizing and corroding atmosphere. Hence, it is widely used in different high-temperature applications, particularly in blades of turbochargers or turbines [1-6]. Inconel superalloys are made through casting, forging, and different heat treatment processes. Microstructural changes which result from different manufacturing processes affect the alloy performance [7]. Thus, the heat treatment process has an important role in achieving optimum microstructure and mechanical properties, such as hardness and creep behavior. Some studies, especially on Inconel-718 superalloy, have focused on these important parameters. In the following paragraphs, these studies have been reviewed.

Kuo et al. [8] studied ageing heat treatment effects on the creep behavior of Inconel-718 superalloy. Their results showed that the amount of δ phase was proportional to the ageing time that affected the creep behavior. Caliari et al. [9] demonstrated that after double heat treatment, creep resistance of Inconel-718 superalloy increased and was affected by γ' and γ'' precipitates and their interactions with dislocations. Chomette et al. [10] investigated the creep behavior of as-received, age-hardened and cold-worked Inconel-617 superalloys. They indicated that the prior 1000 hours thermal ageing heat treatment affected the initial strain rate drop and decreased the creep lifetime. Wen et al. [11] studied the initial ageing time on the processing map and microstructures of a nickel-based superalloy. They found that the ageing heat treatment at 900 °C for 9 hours was suitable for the hammer forging process. Chamanfar et al. [12] claimed that if the solution temperature is increased to 1035 °C and water quenching (instead of air cooling), followed by the double ageing process at 621 °C for 10

*Corresponding Author Email: *m.azadi@semnan.ac.ir* (M. Azadi)

Please cite this article as: M. Azadi, M. Azadi, A. Hajiali Mohammadi, Nitrate Removal from Aqueous Solutions Using Granular Activated Carbon Modified with Iron Nanoparticles, International Journal of Engineering (IJE), IJE TRANSACTIONS A: Basics Vol. 33, No. 4, (April 2020) 639-646

hours is used, the hardness value of 420 Vickers can be obtained. Li et al. [13] studied the effect of different processing technologies and heat treatments on the creep behavior of the GH4169 superalloy. The results showed that the specimen with clean grain boundaries and with no δ precipitates exhibited a much longer creep lifetime. Probstle et al. [14] improved the creep strength of nickel-base superalloys by optimizing the γ/γ' behavior of solid solution strengthening elements. Zhao et al. [15] showed that the microhardness decreased due to the overgrowth of $M_{23}C_6$-type carbides at grain boundaries, with increasing the ageing time. Shin et.al [16] indicated that with increasing the ageing time, the creep lifetime of Ni-based single crystal superalloys reduced. In addition, several studies [1-2, 17-18] investigated the microstructure of the as-cast Inconel-713C superalloy; however, few reports dealt with the relation of the heat treatment and the forging process to mechanical properties of the Inconel-713C superalloy. Thus, the aim of this research is to investigate the creep behavior of the Inconel-713C superalloy after ageing heat treatment without the solutioning step and forging process. Creep parameters under the stress condition of `585.5 MPa and at 850 °C were measured. Then, both the optical microscopy (OM) and the scanning electron microscopy (SEM) techniques were used the microstructural evaluations after the pre-treatment process and creep testing.

2. MATERIALS AND EXPERIMENTS

2. 1. Materials and Pre-Treatment Process Creep-rupture tests were performed on four different types of specimens, made from the Inconel-713C superalloy. The chemical composition (wt.%) of the used material was measured as, C: 0.12%, Cr: 14.00%, Nb: 1.91%, Ti: 0.97%, Al: 5.50%, Fe: 0.13%, Mn: 0.04%, Si: 0.45%, Zr: 0.06%, B: 0.01%, Mo: 4.50%, Cu: 0.01% and balance Ni. The first type was as-cast specimens. The second type of samples was related to the aged-hardened specimens without the solutioning stage. The ageing process contained heating at 930 °C and for 16 hrs. It was noticeable the ageing heat treatment after solutioning process decreased the creep lifetime, with respect to the as-cast sample of the Inconel-713 superalloy [19]. Therefore, the ageing heat treatment without solutioning has been chosen for this research. The third type of samples was the forged specimen. The forging process was done at 1200 °C. The size change of the specimen under the forging process was about 36%. The last type of samples was related to the forged specimen, which was aged- hardened after the forging action, again without the solutioning stage. All specimens were cooled in the ambient air at 25 °C, after heating in the furnace or the forging process.

2. 2. Creep Test Conditions Creep-rupture tests were conducted in accordance with the ASTM-E139, at a temperature of 850 °C. The applied load in all creep testing was constant and the stress value was about 585.5 MPa. This creep condition (the creep stress and temperature) was selected for better comparison of results of this paper with other results in our previous work [18-19]. Details of the utilized creep apparatus used in this study are found in previous works [18-20].

2. 3. Microstructral Evaluation Before and after creep testing, samples were sectioned and polished by using standard metallographic techniques, in accordance with ASTM-E3 and ASTM-E407. Specimens were examined under the OM technique, by the Marble etchant to appear different phases [21]. The grain size measurement was in accordance with the ASTM-E112. The SEM technique (XLC-Philips model) was performed to show the details of microstructures. The energy dispersive spectroscopy (EDS) with the accelerated voltage of 20 kV was also conducted for semi-quantitative chemical analysis of existing phases in different samples. The mean size and mean volume fraction of γ' particles were measured by the MIP-4 student material science and the IMAGE J program.

3. RESULTS AND DISCUSSIONS

3. 1. Microstructral Evaluations before Creep Testing Figure 1(a) shows the microstructure of the as-cast Inconel-713C superalloy, containing the γ matrix with a few granular and lots of intergranular carbides, which were precipitated in the matrix. Alloy carbides were observed in the black-colored region in the OM images. The γ' particles were not clearly seen in the matrix in this image due to their small size; however, they could have appeared in SEM images. Thus, the Inconel-713C superalloy consisted of the γ matrix, alloy carbides, and γ' particles. For the aged- hardened sample, the microstructure changed; the details are shown Figure 1(b). A population of γ' clusters in some areas of the γ matrix can be observed. The γ' clusters or particles accumulation observed in the region as darker-colored than the matrix. They were distributed non-homogeneously in the matrix. In addition, the non-continuous grain boundary carbides and finely dispersed intergranular carbides also appeared in the matrix, according to another research [8]. However, in some areas continuous grain boundary carbides was observed. The microstructure for the forged sample changed completely after36% hot work (forging process) on the specimen. As Figure 1(c) shows, it seemed that the thickness of some alloy carbides has increased. When the forged specimen was aged-hardened, the thickness of

alloy carbides decreased, as shown in Figure 1(d). The γ' clusters were not observed in this specimen with respect to other aged-hardened sample, comparing Figure 1(b) to 1(d).

Figure 2 shows the SEM images of different specimens. In the as-cast sample, a uniform distribution of γ' particles is observed in the matrix. Besides, two types of carbides (MC and $M_{23}C_6$) were found in white- and black-colored regions in the matrix, respectively. The EDS results of the as-cast specimen have been reported in the previous paper [18]. The results demonstrated that MC-type carbides were the NbC ones. A similar result was also reported in other research [8]. By applying ageing heat treatment, the γ' particles were agglomerated in some regions of the matrix. The size of carbides changed significantly, after the ageing heat treatment. The carbide length decreased approximately from 90 μm to 15 μm, as shown in Figure 2(b). When the specimen forged at 1200 °C, the carbide length changed insignificantly with respect to the as-cast specimen. Moreover, a large number of the γ' particles was solutionized or decreased in the γ matrix. No precipitating of $M_{23}C_6$ carbides was observed, since black spots disappeared on the image in Figure 2(c). As the stability temperature of $M_{23}C_6$-type carbides was lower than 1100 °C [22], the forging process could act as a solutioning heat treatment to solutionize these carbides. Kuo et al. [8] reported that after solutioning step, most carbides such as $M_{23}C$-type were dissolved back into the matrix. However, some of the MC-type carbides still remained intact in the matrix. Figure 2 (d) shows that when the forged specimen was aged-hardened, the γ' particles were precipitated in the matrix. It was noticeable that the ageing heat treatment after the forging process reduced the carbide length. However, the morphology of MC carbides changed from the acicular to the rounded shape. More $M_{23}C_6$-type carbides were precipitated in the matrix, among other specimens before creep testing, as shown in Figure 2(d the phase identification of all phases has been conducted by X- ray diffraction patterns (XRD) in some previous studies [19, 23].

For a better discussion, SEM images of the γ' particles plus the γ matrix, before creep testing, which was edited by the IMAGE J program are shown in Figure 3. For the as-cast specimen, the mean size of the γ' particles was 800 nm. The morphology of this phase was the rounded shape. When the specimen age-hardened, the amount of the γ' particles changed, as reported in Table 1. The γ' particle size increased to 1000 nm, due to the coalescence of particles. The morphology of the γ' particles changed to a semi-cubical shape. It was found that the transition of the γ' particles shape in the matrix, from spherical to cuboidal, occurred when the γ' particles size became large [24]. Thus, the microstructure of the age-hardened superalloy consisted of the cubical γ' phase, embedded in the γ matrix. As the ageing time increased from 200 to 800 hours, the morphology of the γ' phase changed from the spherical to the cubic shape [16]. Therefore, such changes (the γ' particles size and the volume percent) for 16 hours seemed to be logical. When the specimen was forged at 1200 °C, the size and the amount of the γ' phase decreased drastically to 250 nm and 22 volume percent, respectively. In this situation, the decrease in the γ' volume fraction in the forged specimen was acceptable. The ageing heat treatment after the forging process increased the amount of γ' particles with a value of 53.8 volume percent. In addition, the size of this phase increased to 400 nm. It was found that the γ'

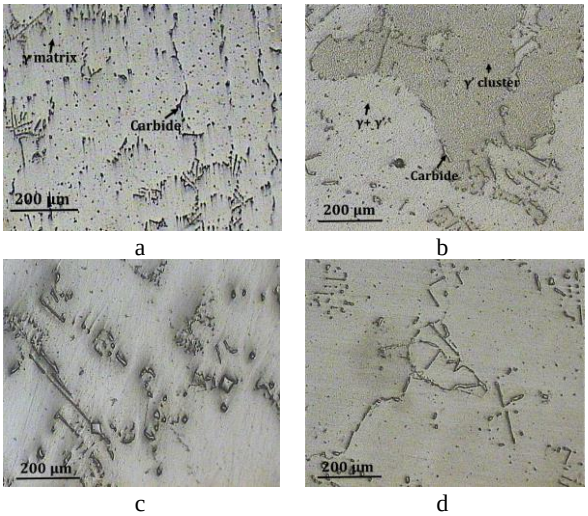

Figure 1. Microstructures of all specimens before creep testing; including (a) as-cast, (b) age-hardened specimen as-cast, (c) forged, and (d) age-hardened forged

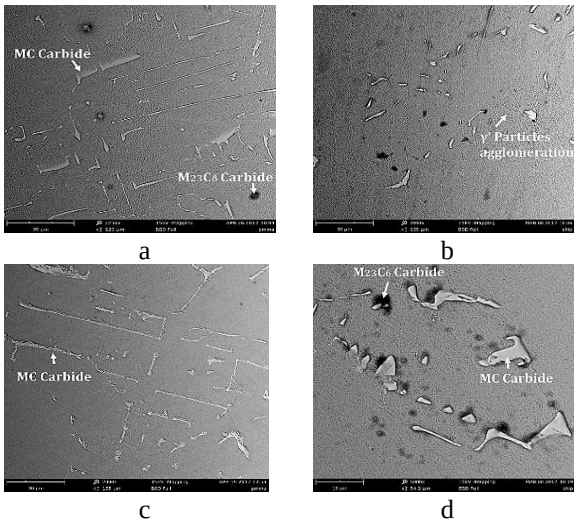

Figure 2. SEM images of all specimens before creep testing; including (a) as-cast specimen (b) age-hardened as-cast (c) forged and (d) age-hardened forged

particles fraction measurements were done in two-dimension. In addition, the mean grain size of this sample increased 25% after the forging process, as reported in Table 1.

3. 2. Creep Testis Results In Figure 4, curves of the engineering strain versus the creep time are shown for all specimens.

All samples, except the forged specimen, showed a typical creep behavior containing the three regimes. However, the forged specimen indicated a diverse creep behavior, under the same creep condition. According to Table 1 and Figure 4, the ageing process increased the secondary stage of the creep rate about 3 times with respect to the as-cast specimen. The rupture lifetime was also reduced by 40%, comparing to the as-cast specimen. The creep strain also increased from 0.10 to 0.15, by the ageing heat treatment. It is noticeable that when the γ' particles precipitated in clusters and agglomerated in some regions by the ageing process, more dislocations migrated easily in the γ matrix channel and the decrease in the creep lifetime and the increase in the creep strain could have happened [25]. In addition, the γ' shape affected the alloy strength. The lattice misfit would be increased when the γ' particle shape changed from spherical to semi-cubical form. Such behavior could also reduce the creep lifetime [25]. Thus, increasing the lattice misfit in the γ' shape in such specimen could be another reason for lowering the creep lifetime. Although the ageing heat treatment after the forging process minimized the creep rate at the secondary stage, the creep lifetime decreased by 64%, with respect to the as-cast sample. This event depicted that the tertiary stage was started earlier for this specimen, comparing to the as-cast one. The lowest creep rate was also attributed to the precipitation of fine intergranular carbides on slip lines, which pinned dislocations, as the hardening effect [10].

It was found that the existence of fine γ' particles in the matrix and the small grain size of the alloy were responsible for lowering of the creep rate [21]. The forged specimen showed the sigmoidal creep behavior since the creep rate increased after the primary regime. This strain rate enhancement led to a jump directly to the tertiary creep regime, in the absence of a steady state creep stage. In other words, in this situation, the strain increased linearly by increasing the time, which was not common for the creep behavior of superalloys. This behavior demonstrated that the work hardening in this specimen was not dominated and the creep lifetime decreased with respect to other specimens. In the first

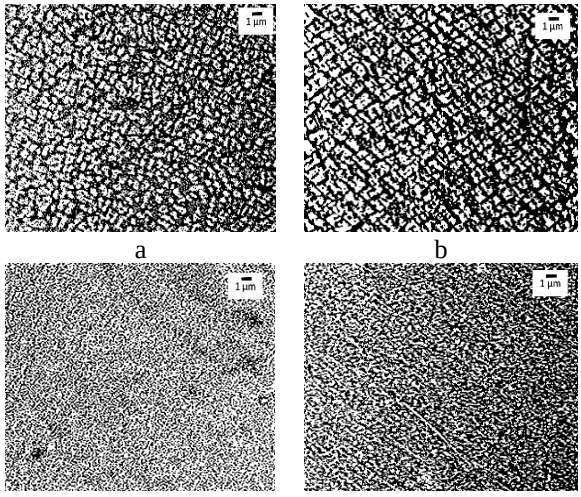

Figure 3. SEM images of γ'+ γ for all specimens before creep testing; which were edited by the IMAGE J program; including (a) as-cast, (b) age-hardened as-cast, (c) forged, and (d) age-hardened forged

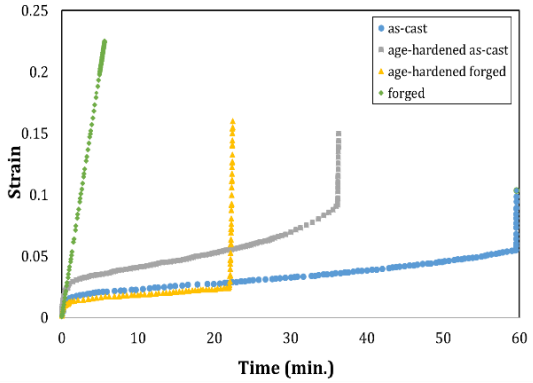

Figure 4. Curves of the engineering strain versus the creep time for all specimens

TABLE 1. Different measurements for all specimens

Specimens type	As-cast	Age-hardened as-cast	Forged	Age-hardened forged
Rupture time (s)	3576	2177	337	1345
Fracture strain	0.10	0.15	0.22	0.16
Creep rate (min^{-1})	0.0004	0.0014	-	0.0003
Mean size of γ' particles (nm) before creep testing	800	1000	250	400
Mean size of γ' particles (nm) after creep testing	500	700	200	300
Mean volume fraction of γ' particles before creep testing	52.5±2.0	54.5±2.0	22.0±2.0	53.8±2.0
Mean grain size (μm)	120±5.0	125±5.0	80±5.0	100±5.0

stage of the creep deformation, the stress increased sharply due to the dislocation generation and the multiplication in the forged sample. However, the ageing heat treatment after the forging process changed the dislocation density. The lower density of dislocation could postpone the softening process and also postponed the second stage of the creep rate. In addition, the highest creep strain with a value of 0.22 for the forged specimen could be the result of the low size of the γ' particles.

3. 3. Microstructral Evaluations after Creep Testing In Figure 5, OM images of ruptured surfaces in different specimens are shown.

Figure 5(a) depicts that carbides were elongated in the same direction to the applied stress. According to Table 1, the γ' particle size decreased from 800 nm to 500 nm. This behavior was related to the interaction of the moving dislocation with the γ' particles. A similar observation has been reported elsewhere [20]. The microstructure of the ruptured age-hardened specimen was different from that of the as-cast specimen, comparing Figure 5(a) to 5(b), and the γ' clusters were broken and distributed in the matrix, uniformly. The γ' particle size decreased from 1000 nm to 700 nm, as shown in Table 1. Figure 5(c) indicates the small size of alloy carbides after creep testing with the value of 20 μm. Grain boundaries in this image were clearly seen, as well. The grain size was 80 μm. It was noticeable that Mei et al. [4] also showed that after the solution treatment at 1200 °C for 1 hr, the heterogeneous equiaxed grains structure obtained with an average grain size of 65 μm. Since grain size changes before and after creep testing were insignificant for all specimens due to the short-term creep testing, one-grain size value was reported in Table 1 for each sample. It was found that the γ' particle size decreased to 200 nm, after creep testing, as presented in Table 1. It was found that the grain boundary sliding could be also activated during creep testing when the grain size of the alloy was small [8]. Therefore, such an event would reduce the creep lifetime. In Figure 5(d), the amount of carbides with the maximum size of 100 μm was uniformly dispersed in the matrix, which was NbC according to the EDS results shown in Table 2. After creep testing, the γ' particle size of the alloy did not show any growth, as the temperature of the testing was lower than the solution temperature of the γ' phase [26]. Due to the results in Table 1, the γ' particle size decreased from 400 nm to 300 nm, after creep testing. Thus, there was a moderate dependence of the creep rupture strength on the γ' particles size. Similar to this paper results, Shingledecker et al. [21] reported that the optimum value of the γ' particle size (800 nm) improved the creep rupture lifetime.

Figure 6 presents SEM images of different specimens in the longitudinal direction.

Figure 6(a) shows elongated MC-type carbides, which were rich in Nb (the chemical composition is shown in Table 2), in the white-colored region, after creep testing. Plus the MC-type carbides, $M_{23}C_6$-type carbides were found in the microstructure which is seen in the black-colored region. The $M_{23}C_6$-type carbides were rich in Cr and Ni (the chemical composition is shown in Table 2). The amount of these carbides increased after creep testing. This event indicated that the high value of the applied stress during creep testing led the reaction of $MC + \gamma \rightarrow M_{23}C_6 + \gamma'$ to occur at lower temperatures. This reaction could be done thermodynamically at temperatures higher than 1000 °C. However, the existence of the applied stress decreased the reaction temperature as low as 850 °C [21]. As shown

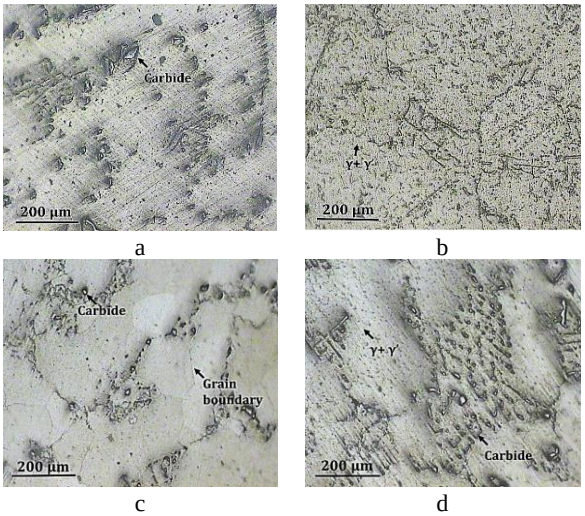

Figure 5. OM images of all specimens after creep testing; including (a) as-cast, (b) age-hardened as-cast, (c) forged, and (d) age-hardened forged

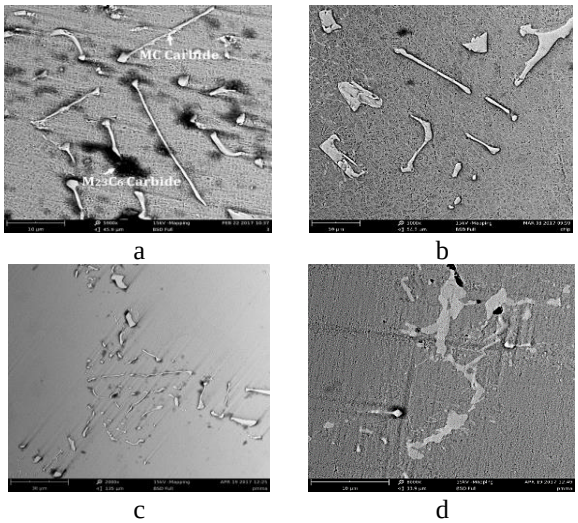

Figure 6. SEM images of all specimens after creep testing in the longitudinal direction; including (a) as-cast, (b) age-hardened as-cast, (c) forged, and (d) age-hardened forged

in Figure 6(b), the amount of $M_{23}C_6$-type secondary carbides in the age-hardened specimen was lower than the as-cast specimen. This behavior was due to the lower creep time duration. Chomette et al. [11] reported that when $M_{23}C_6$-type secondary carbides could be precipitated on slip planes during creep testing, they were useful in increasing the creep lifetime of the alloy. Thus, the highest creep lifetime of the as-cast specimen could be attributed to have the highest amount of $M_{23}C_6$-type carbides participation during creep testing. In addition, MC-type carbides were also seen in the elongated shape, similar to the as-cast specimen. Grain boundaries were decorated with thick planar $M_{23}C_6$-type carbides that increased the creep lifetime of the alloy [10]. In the forged specimen, $M_{23}C_6$-type carbides were not seen after creep testing, as shown in Figure 6(c). When the forged specimen was age-hardened, the small amount of $M_{23}C_6$-type carbides plus MC-type carbides appeared in the matrix, as shown in Figure 6(d). The γ' phase volume percent decreased about 45% (the highest value) after creep testing.

The EDS results for various specimens after creep testing are reported in Table 2. According to Table 2, no new phase precipitated from the γ matrix, during creep testing. The γ matrix was a solid solution phase that contained several elements such as Fe, Cr, Mo, and Ti. The high solubility of many elements could strengthen the γ matrix. The γ' phase with the chemical composition of Ni_3(Al, Ti) and with a cubic crystal structure also had a high volume, compared to its mass. This phase had strong attractive bonds with various atoms and therefore, exhibited specific mechanical properties [21]. Two types of MC-type carbides (with the NaCl-type structure) and $M_{23}C_6$-type carbides were also observed. MC-type carbides had the lattice constant of 0.40 nm and $M_{23}C_6$-type carbides had the lattice constant of 0.43 nm. $M_{23}C_6$-type carbides were rich in Cr. In some cases, the eutectic phase and MC_6-type carbides were formed in Inconel microstructures [16]. However, these phases did not observe in this research.

TABLE 2. The EDS results of different phases (% wt)

Element	MC	$M_{23}C_6$	γ'+ γ
Nb	40.8	1.2	1.5
Ni	16.3	15.4	63.0
Ti	11.0	3.1	2.4
Mo	8.7	2.8	2.9
C	11.1	36.3	4.8
Cr	5.6	34.4	14.7
Al	4.7	5.7	10.0
Mn	0.5	0.4	0.2
Fe	1.3	0.7	0.5

3. 4. Fracture Analysis To identify creep failure mechanisms, fractoghraphs of ruptured surfaces for different specimens were characterized by means of SEM. As shown in Figure 7(a), in the as-cast specimen, slip planes were weaker than grain boundaries and cleavages in different slip planes were observed. There were small quadrilateral cleavage planes in different areas of the ruptured surface and cracks propagated around these cleavage planes. Such fractographic images were also found in other researches [27]. For the age-hardened specimen, the transgranular micro-pores coalescence observed at the intersection of grains, as depicted in Figure 7(b). Vacancies clusters at grain boundaries under stress concentration sites created micro-pores [28]. However, when the specimen was forged, the intergranular fracture was the predominated mechanism due to the crack growth in grain boundaries. In this situation, grain boundaries were weaker than slip planes. Moreover, the existence of cracks would be attributed to carbides participations which were segregated at grain boundaries prior to failure. Decreasing of the grains size in the forged specimen also observed obviously in Figure 7(c). It was found that the grain boundary sliding increased the creep strain and reduced the creep lifetime when the grain size of the alloy was small [8]. In addition, there was no obvious creep cavitation on the surface image of the ruptured specimen. Thus, the mobility of dislocations rather than creep cavitation would be the dominant mechanism for increasing the tertiary stage of the creep rate. When the forged specimen were aged-hardened, the formation of more micro-pores was likely possible, as shown in Figure 7(d). The micro-pore formation usually happened between the boundaries of the γ' and the γ phases. The generation of these micro-pores acted as nuclei sites for

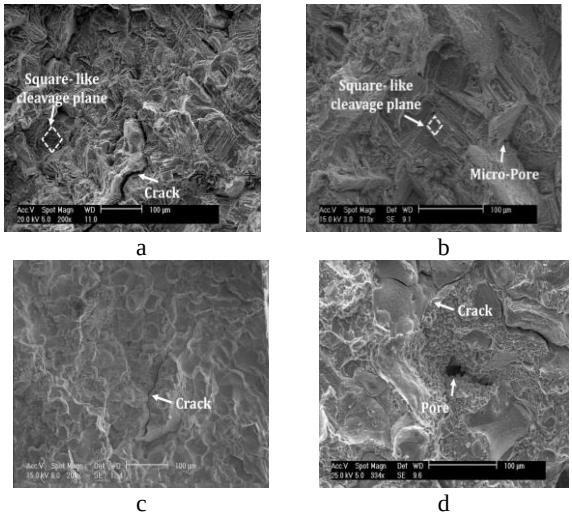

Figure 7. Fracture surface images of all ruptured specimens; including (a) as-cast, (b) age-hardened as-cast, (c) forged, and (d) age-hardened forged

the crack growth initiation, as reported by other research [28, 29]. Consequently, the fracture surface of forged specimens (whether initial or age-hardened ones) showed to be more brittle than as-cast specimens (whether initial or age-hardened ones).

4. CONCLUSIONS

In this study, the short-term creep behavior of as-cast and forged specimens made of the Inconel-713C superalloy was investigated. In addition, effects of the ageing heat treatment without the solutioning stage on creep properties and microstructural aspects were studied. Outstanding results were as follows,

- Due to the decrease in the amount of $M_{23}C_6$-type secondary carbides precipitation, the ageing heat treatment could not increase the creep rupture lifetime of the Inconel-713C superalloy with respect to the as-cast specimen. However, the ageing heat treatment increased the creep lifetime (4 times) of the forged specimen.
- The ageing heat treatment at 930 °C for 16 hours promoted the growth of the γ' phase in the cluster, from 800 to 1000 nm. Besides, the shape of γ' particles changed from rounded to semi-cubical phase. Such behavior shortened the creep lifetime by 40%, with respect to the as-cast specimen.
- The γ' particle size was more effective than the amount of the γ' phase. The optimum size of the γ' particle was 800 nm to increase the short-term creep lifetime. The lower size of γ' particle (200 nm) could not also increase the creep lifetime.
- Grain boundaries cracks on the ruptured surface were more obvious for the forged specimen due to the decrease in the grain size, during the hot forging process.

5. REFERENCES

1. Zupanic, F., Boncina, T., Krizman, A., Tichelaar, F.D., "Structure of continuously cast Ni-based superalloy Inconel 713C", ***Journal of Alloys and Compounds***, Vol. 329, (2001), 290-297.
2. Azadi, M., Iziy, M., Marbout, A., Azadi, M., Rizi, M.H., "Investigation of the heat treatment effect on microstructures and phases of inconel 713c superalloy", ***International Journal of Engineering Transaction A: Basics***, Vol. 30, No. 10, (2017) 1538-1544.
3. Lee, J.W., Kim, D.J., Hong, H.U., "A new approach to strengthen grain boundaries for creep improvement to a Ni-Cr-Co-Mo superalloy at 950°C", ***Materials Science and Engineering A***, Vol. 625, (2015), 164-168.
4. Mei, Y., Liu, Y., Liu, C., Li, C., Yu, L., Guo, Q., Li, H., "Effects of cold rolling on the precipitation kinetics and the morphology evolution of intermediate phases in Inconel 718 alloy", ***Journal of Alloys and Compounds***, Vol. 649, (2015), 949-960.
5. Dirbude, S.B., Maurya, V.K., "Effect of uniform magnetic field on melting at various rayleigh numbers", ***Emerging Science Journal***, Vol. 3, No. 4, (2019), 263-273.
6. Su, Y., Li, X., Wu, X., "Evaluation of load-bearing performance of existing cast steel node", ***Civil Engineering Journal***, Vol. 3, No. 2, (2017), 88-94.
7. Azadi, M., Iziy, M., Marbout, A., Azadi, M., Hajiali Mohammadi A., "Optimization of solution temperature and time in nickel-based super-alloy of engine turbo-charger based on hardness by design of experiments", ***The Journal of Engine Research***, Vol. 43, (2016), 63-70.
8. Kuo, C.M., Yang, Y.T., Bor, H.Y., Wei, C.N., Tai, C.C., "Aging effects on the microstructure and creep behavior of Inconel 718 superalloy", ***Materials Science and Engineering A***, Vol. 510-511, (2009), 289-294.
9. Caliari, F.R., Candioto, K.C.G., Couto, A.A., Nunes, C.N., Reis, D.A.P., "Effect of double aging heat treatment on the short-Term creep behavior of the Inconel 718", ***Journal of Materials Engineering and Performance***, Vol. 25, (2016), 2307-2317.
10. Chomette, S., Gentzbittel, J.M., Viguier, B., "Creep behavior of as received, aged and cold worked Inconel 617 at 850 °C and 950 °C", ***Journal of Nuclear Materials***, Vol. 399, (2010), 266-274.
11. Wen, D.X., Lin, Y.C., Chen, J., Deng, J., Chen, X.M., Zhang, J.L., He, M., "Effects of initial aging time on processing map and microstructures of a nickel-based superalloy", ***Materials Science and Engineering A***, Vol. 620, (2015), 319-332.
12. Chamanfar, A., Sarrat, L., Jahazi, M., Asadi, M., Weck, A., Koul, A.K., "Microstructural characteristics of forged and heat treated Inconel-718 disks", ***Materials and Design***, Vol. 52, (2013), 791-800.
13. Li, H.Y., Kong, Y.H., Chen, G.S., Xie, L.X., Zhu, S.G., Sheng, X., "Effect of different processing technologies and heat treatments on the microstructure and creep behavior of GH4169 superalloy", ***Materials Science and Engineering A***, Vol. 582, (2013), 368-373.
14. Probstle, M., Neumeier, S., Feldner, P., Rettig, R., Helmer, H.E., Singer, R.F., Goken, M., "Improved creep strength of nickel-base superalloys by optimized γ/γ′ partitioning behavior of solid solution strengthening elements", ***Materials Science and Engineering A***, Vol. 676, (2016), 411-420.
15. Zhao, X., Dang, Y., Yin, H., Yuan, Y., Lu, J., Yang, Z., Gu, Y., "Evolution of the microstructure and microhardness of a new wrought Ni–Fe based superalloy during high temperature aging", ***Journal of Alloys and Compounds***, Vol. 644, (2015), 66-70.
16. Shin, Z., J. Li, S. Liu, "Effect of long term aging on microstructure and stress rupture properties of a nickel based single crystal superalloy", ***Progress in Natural Science: Materials International***, Vol. 22, (2012), 426-432.
17. Pokluda, J., Obrtlik, K., Slamecka, K., Hornikova, J., Kianicova, M., "Fatigue life of cast Inconel 713LC with/without protective diffusion coating under bending", torsion and their combination, ESIS TC2 (Micro mechanisms), Oxford (2012)
18. Azadi, M., Azadi, M., "Evaluation of high-temperature creep behavior in Inconel-713C nickel-based superalloy considering effects of stress levels", ***Materials Science and Engineering A***, Vol. 689, (2017), 298-305.
19. Azadi, M., Marbout, A., Safarloo, S., Azadi, M., Shariat, M, Rizi, M.H., Effects of solutioning and ageing treatments on properties of Inconel-713C nickel-based superalloy under creep loading", ***Materials Science and Engineering A***, Vol. 711, (2018), 195-204.
20. Bahmanabadi, H., Rezanezhad, S., Azadi, M., Azadi, M., "Characterization of creep damage and lifetime in Inconel-713C nickel based superalloy by stress-based, strain/strain rate-based and continuum damage mechanics models", ***Materials Research Express***, Vol. 5, (2018), 026509.
21. Shingledecker, J.P., Evans, N.D., Pharr, G.M., "Influences of composition and grain size on creep-rupture behavior of Inconels

alloy740", ***Materials Science and Engineering A***, Vol. 578, (2013), 277-286.

22. Bhambri, A.K., Kattamis, T.Z., Morral, J.E., "Cast microstructure of Inconel 713C and its dependence on solidification variables", ***Metallurgical Transaction B***, Vol. 6, (1975), 523-537.
23. Safarloo, S., Loghman, F., Azadi, M., Azadi, M., "Optimal design experiment of ageing time and temperature in inconel-713C superalloy based on hardness objective", ***Transactions of the Indian Institute of Metals***, Vol. 71, (2018), 1563-1572.
24. Yu, L.H., Ping, S.X., Li, W.Y., Liang, C.G., "Coarsening and age hardening behaviors of γ' particles in GH742 during high temperature treatment, ***Journal of Iron and Steel Research***, Vol. 16, (2009), 81-86.
25. Murakumo, T., Koizumi, Y., Kobayashi K., Harada, H., "Creep strength of Ni-base single-crystal superalloys on the γ/ γ tie- line", ***Minerals, Metals and Materials Society***, Vol. 2004, (2004), 155-163.
26. Ji, C.L., Ge, C.C., Yan, Q.Z., "Microstructure evolution and mechanical properties of disk superalloy under multiplex heat treatment", ***Materials Science and Engineering A***, Vol. 659, (2016), 287-294.
27. Shi, D., Dong, C., Yanga, X., Zhang, L., Hou, J., Liu, Y., "Experimental investigations on creep rupture strength and failure mechanism of vacuum brazed joints of a DS superalloy at elevated temperature", ***Materials Science and Engineering A***, Vol. 545, (2012), 162-167.
28. Sun, F., Gu, Y.F., Yan, J.B., Xu, Y.X., Zhong, Z.H., Yuyama, M., "Creep deformation and rupture mechanism of an advanced wrought Ni-Fe-based superalloy for 700 °C class A-USC steam turbine rotor application", ***Journal of Alloys and Compounds***, Vol. 687, (2016), 389-401.
29. Iziy, M., Azadi, M., Marbout, A., Rizi, M.H., Azadi, M. "The effect of heat treatment temperature on superalloy Inconel 713 hardness and microstructure", ***Metallurgical Engineering***, Vol. 19, No. 2, (2016), 124-134.

Persian Abstract

چکیده

در این مقاله، رفتار خزشی کوتاه‌مدت سوپرآلیاژ اینکونل ۷۱۳C پس از پیش‌عملیات‌های مختلف شامل فرآیند پیرسازی و آهنگری در دمای ۸۵۰ درجه‌ی سانتی‌گراد بررسی شد، . عملیات حرارتی پیرسازی شامل گرمایش در دمای ۹۳۰ درجه‌ی سانتی‌گراد به مدت ۱۶ ساعت بدون فرایند محلول‌سازی بود. فنون میکروسکوپ نوری و میکروسکوب الکترونی رویشی برای ارزیابی میکروساختاری استفاده شد.. نتایج حاصل نشان داد که علی‌رغم این که عملیات پیرسازی میزان فاز γ' را افزایش داد، آلیاژ پیرسخت‌شده دارای عمرخزشی کمتر (حدود ٤٠ درصد) نسبت به آلیاژ ریخته‌گری‌شده بود. این رویداد به دلیل کاهش مقدار رسوبات کاربیدی نوع دوم $M_{23}C_6$ است. زمانی که سوپرآلیاژ اینکونل ۷۱۳C در دمای ۱۲۰۰ درجه‌ی سانتی‌گراد آهنگری شد، مرحله‌ی سوم نمودار خزش (کرنش-زمان) به صورت چشم‌گیری افزایش یافت و عمرخزشی را کاهش داد. اندازه‌ی دانه‌ی کوچک نمونه‌ی آهنگری‌شده موجب چنین رفتار معکوس خزشی شد. به علاوه، شکست‌نگاری این نمونه نشان داد که ترک‌های بین‌دانه‌ای روی سطح شکست وجود داشت. هنگامی که نمونه آهنگری‌شده بدون عملیات محلول‌سازی پیرسازی شد، عمرخزشی آن نسبت به نمونه‌ی آهنگری‌شده ٤ برابر افزایش یافت.